AUTOMATIC HUMAN BRAIN VESSEL SEGMENTATION FROM 3D 7 TESLA MRA IMAGES USING FAST MARCHING WITH ANISOTROPIC DIRECTIONAL PRIOR

Wei Liao[1], *Karl Rohr*[1], *Chang-Ki Kang*[2], *Zang-Hee Cho*[2], *and Stefan Wörz*[1]

[1]University of Heidelberg, BIOQUANT, IPMB, and DKFZ Heidelberg
Dept. Bioinformatics and Functional Genomics, Biomedical Computer Vision Group
Im Neuenheimer Feld 267, 69120 Heidelberg, Germany. E-mail: wei.liao(at)bioquant.uni-heidelberg.de
[2]Neuroscience Research Institute, Gachon University of Medicine and Science
Namdonggu, Incheon, 405-760, Republic of Korea

ABSTRACT

Accurate 3D models of the human brain vessels can greatly help to diagnose serious diseases. Such models can be constructed by segmentation of 3D MRA images, especially the recently introduced high resolution 7T MRA. We propose a new two-step approach for fully automatic segmentation of 7T MRA images of the human cerebrovascular system. First, a 3D model-based approach is applied to segment thick vessels and most parts of thin vessels. Then, the missing vessel parts, which are caused by low contrast and high noise, are completed using a novel fast marching approach with anisotropic directional prior. An evaluation of our approach and a comparison with two previous approaches have been conducted using high resolution 3D 7T MRA images.

Index Terms— Automatic 3D segmentation, Cerebral vasculature, 7T MRA, anisotropic fast marching

1. INTRODUCTION

Analysis of human brain vessels is important for the diagnosis of many serious diseases such as stroke. For such an analysis, accurate 3D models are very useful, which can be created by 3D segmentation of magnetic resonance angiography (MRA) images. With the recently introduced 7 Tesla (7T) MRA, much more vessels, especially thin vessels, are visible than with 1.5T or 3T MRA [1], but the signal-to-noise ratio is only slightly higher [2]. Furthermore, the human brain vasculature system is highly complex, e.g., see Fig. 1 (left) for a maximum intensity projection (MIP) of a region. Thus, segmentation is a very difficult task. In [2], the segmentation is performed manually, which is very time consuming and not suitable for a large number of images. Therefore, automatic segmentation is required.

For vessel segmentation of 3D medical images, different approaches exist. For example, approaches based on *deformable models* represent the contour or intensity profile of vessels (e.g., [3]). For these approaches, segmenting vessels in regions with low contrast and high noise remains difficult.

Another class of approaches is based on *minimal paths*, where the path between given start and end points with minimum cost is computed. In minimal path approaches based on the *Dijkstra's algorithm* (e.g., [4, 5, 6]), vesselness measures (e.g., [7]) are often used to construct graphs, but it is difficult to prefer specific directions, and one remedy is to discard vessel candidates deviating too much from given directions [5]. In [6], undesired directions are not discarded, but penalized with a higher cost. However, an inherent problem of Dijkstra's algorithm is the *metrication error* [8], caused by the discrete graph structure.

In contrast, minimal path approaches based on *fast marching* avoid metrication errors by using a continuous formulation [8]. However, with the traditional fast marching method, it is difficult to prefer specific directions because the numerical scheme assumes an isotropic metric [9]. This problem has been addressed by anisotropic fast marching approaches. However, these approaches are computationally expensive, and different approximations are used in practice [9, 10], which are still less efficient than the isotropic version.

In a minimal path approach based on *sampling* [11], each path is regarded as a sample from a generative model, and each sample is assessed by an energy function. By systematically drawing samples a number of times, the sample with minimum energy is selected. However, for long paths, too many samples are needed to guarantee a reasonable result. Furthermore, when processing the same image, the results differ slightly due to the probabilistic nature of this approach.

We introduce a new two-step approach for automatic segmentation of human brain vessels from high resolution 3D 7T MRA images. In the first step, a robust model-based approach [3] is used to segment most vessels up to some gaps between them. These gaps are completed in the second step using a novel fast marching approach with an anisotropic directional prior. In contrast to previous work (e.g., [4, 5, 6, 11]), our approach avoids metrication errors, and allows using prior knowledge about the vessel direction, which helps to segment vessels in regions with low contrast and high noise. The anisotropic prior is integrated as a soft constraint. However, in contrast to previous anisotropic fast marching approaches [9, 10], we integrate the anisotropic prior into an *isotropic* fast marching method, which avoids high computational costs. In contrast to [11], our approach is deterministic, while being

computationally much more efficient. Furthermore, our approach allows to quantify relevant properties like the vessel length, and it is fully automatic.

2. 3D TWO-STEP VESSEL SEGMENTATION

Our approach for segmentation of vessels from 3D 7T MRA images consists of two steps. First, thick vessels and most thin vessels are segmented using a model-based approach. Second, a novel fast marching approach is used to automatically complete the remaining gaps of the segmentation result.

2.1. 3D Model-Based Approach

Thick vessels and most of the thin vessels can be well segmented using a *3D parametric intensity model* [3]. The model represents the intensity profile and shape of vessels within a 3D region of interest (ROI) by using an ideal sharp 3D cylinder convolved with a 3D Gaussian. Furthermore, a 3D rotation and translation are also incorporated. To segment a *vessel segment*, the model is directly fitted to the image data using least-squares fitting within the ROIs. To segment a *complete vessel*, a Kalman filter is applied to estimate the location of the next ROI along a vessel. For segmentation of *all vessels*, we use an automatic initialization scheme [11] based on a vesselness map and eigenvectors of the Hessian matrix. As a result of the model-based approach, the 3D position, radius, and direction at each centerline point of a vessel are estimated, and all voxels belonging to vessels are masked.

2.2. Fast Marching Approach With Anisotropic Directional Prior

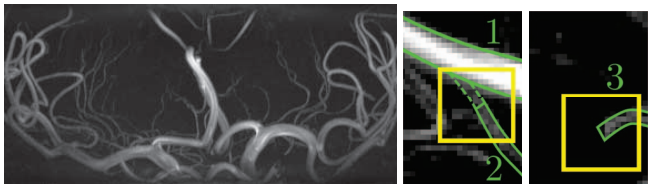


Fig. 1. Left: MIP of one 3D 7T MRA image of human brain vessels. Middle and right: Sections of the MIP of a region of the brain. The results of the model-based approach (solid contours) and FM-ADP (dashed contours) and the corresponding ROIs (yellow boxes) are highlighted for three vessels.

Thick vessels and most of the thin vessels can be segmented correctly using the model-based approach described above. However, in the proximity of thick vessels, thin vessel ends may not be segmented due to low contrast and high noise. This is illustrated in Fig. 1 (middle). There, vessel 2 has not been connected to the thick vessel 1. To complete those gaps, we employ a fast marching approach with anisotropic directional prior (FM-ADP). For each vessel, the start point $\mathbf{x}_\mathrm{m}$ is the last point of the result from the model-based approach, while the set of possible end points $\mathcal{E}$ are voxels which are masked as vessel by the model-based approach and are contained in a cubic ROI centered around $\mathbf{x}_\mathrm{m}$ (yellow box in Fig. 1, middle). If $\mathcal{E} = \emptyset$, then there are no thick vessels nearby and thus no connection is needed. For example, in Fig. 1 (right), the end of vessel 3 should not be connected to other vessels. If $\mathcal{E} \neq \emptyset$, our goal is to find the vessel *centerline* as the minimal path connecting $\mathbf{x}_\mathrm{m}$ to any point in $\mathcal{E}$. In our approach, we assume that the vessel in each completed gap has constant radius equal to the radius of the last segment quantified by the model-based approach. In the following, we first review the standard fast marching approach. Then, we introduce an extension with an anisotropic directional prior.

2.2.1. Standard Fast Marching Approach

Given a start point and an end point, fast marching aims at finding the path l minimizing the energy function

$$E(l) = \int_l (\mathcal{P}(s) + \epsilon)\, ds, \tag{1}$$

where $\mathcal{P}$ is a potential function derived from an image, ϵ is a constant regularization term which controls the smoothness of the path, and s is the arc length parameter. $\mathcal{P}$ can be interpreted as the inverse of the propagation speed $\mathcal{F}$ of a wavefront emanating from the start point:

$$\mathcal{P}(s) = \frac{1}{\mathcal{F}(s)}. \tag{2}$$

The optimal path minimizing the energy (1) can be found by solving the Eikonal equation, defined using an action map $\mathcal{U}$, which describes the arrival time of the wavefront at $\mathbf{x}$:

$$\|\nabla \mathcal{U}(\mathbf{x})\| = \mathcal{P}(s) + \epsilon. \tag{3}$$

Note that this equation employs the Euclidean norm of the gradient $\|\nabla \mathcal{U}(\mathbf{x})\|$, which is the same for all directions, i.e., the speed function must be *isotropic*.

2.2.2. Anisotropic Directional Prior

The model-based approach provides an estimate of the tangent $\mathbf{d}_\mathrm{m}$ at each start point $\mathbf{x}_\mathrm{m}$, which can be used to disambiguate vessels in regions with low contrast and high noise. Obviously, $\mathbf{d}_\mathrm{m}$ involves anisotropic information, which may suggest using an anisotropic fast marching approach. However, below we show that it is possible to incorporate $\mathbf{d}_\mathrm{m}$ into the *isotropic* Eikonal equation. Our idea is illustrated

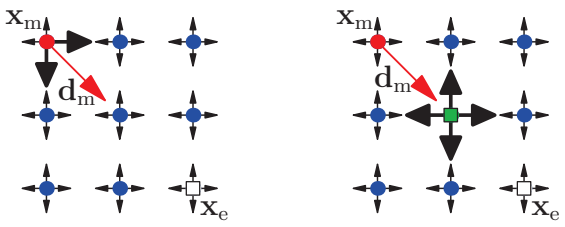
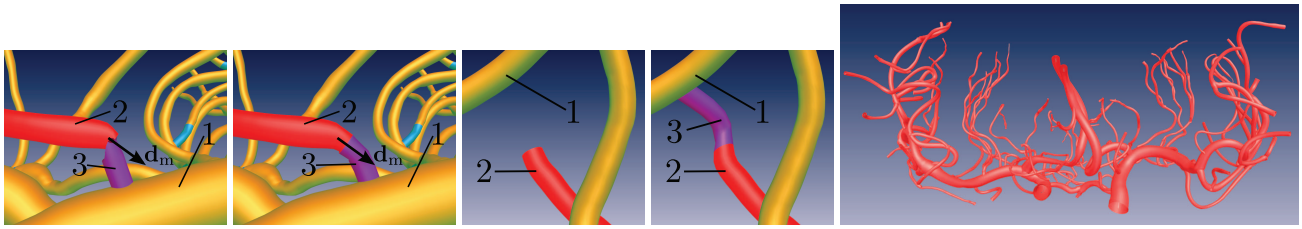


Fig. 2. 2D sketch of 3D anisotropic effect: using anisotropic speed (left) and isotropic speed (right).



(a) FM-V (b) our approach (c) PROB [11] (d) our approach (e)

Fig. 3. (a), (b) Results of FM-V and our approach for a gap with high curvature, (c), (d) Results of PROB [11] and our approach for a large gap. Label 1: thick vessel, 2: result of model-based approach (red), 3: completed gap (magenta), (e) Final result.

in Fig. 2. There, each dot or square represents a voxel, and the start point $\mathbf{x}_\mathrm{m}$ and end point $\mathbf{x}_\mathrm{e}$ are highlighted as red dots and white squares, respectively. The initial direction $\mathbf{d}_\mathrm{m}$ is indicated as a red arrow. The black arrows show the speed at voxels in different directions. Suppose that we prefer paths such that the initial tangents of the paths point in directions similar to $\mathbf{d}_\mathrm{m}$. Using an anisotropic speed (Fig. 2, left), this can be achieved by increasing the speeds in specific directions at $\mathbf{x}_\mathrm{m}$ (large arrows). However, such an anisotropic speed cannot be handled using the isotropic Eikonal equation. The idea in our approach is that a similar anisotropic effect can be achieved using an *isotropic* speed. Instead of increasing the speed in preferred *directions*, we increase the *isotropic* speed at preferred *image points*. For example, in Fig. 2 (right), all speeds in the different directions at the green voxel are increased to the same large value. On the scale of the whole image, an anisotropy is achieved, i.e., the paths passing through the green voxel are preferred, but on the scale of individual voxels, this speed function is still isotropic, and consequently the *isotropic* Eikonal equation can be applied. To integrate the anisotropy, we propose the following energy function as an extension of (1):

$$E(l, \mathbf{x}_\mathrm{m}, \mathbf{d}_\mathrm{m}) = \int_l \Big(\mathcal{P}_\mathrm{comp}(s, \mathbf{x}_\mathrm{m}, \mathbf{d}_\mathrm{m}) + \epsilon\Big) ds, \quad (4)$$

where the new composite potential function is defined as:

$$\mathcal{P}_\mathrm{comp}(s, \mathbf{x}_\mathrm{m}, \mathbf{d}_\mathrm{m}) = \frac{1}{\mathcal{F}_\mathrm{v}(s) + w \cdot \mathcal{F}_\mathrm{dir}\Big(\mathbf{x}(s) - \mathbf{x}_\mathrm{m}, \mathbf{d}_\mathrm{m}\Big)}. \quad (5)$$

$\mathcal{P}_\mathrm{comp}$ includes a speed function $\mathcal{F}_\mathrm{v}$ based on a multiscale vesselness filter as well as a speed function $\mathcal{F}_\mathrm{dir}$ based on an anisotropic directional prior which are detailed below (w is a scalar weight).

2.2.3. *Speed Function $\mathcal{F}_\mathrm{v}$*

The speed function $\mathcal{F}_\mathrm{v}$ is defined as:

$$\mathcal{F}_\mathrm{v}(s) = \max_{\sigma_\mathrm{min} \le \sigma \le \sigma_\mathrm{max}} \mathcal{V}_\sigma(\mathbf{x}). \quad (6)$$

In our approach, the filter from [7] is used, i.e., $\mathcal{V}_\sigma(\mathbf{x}) =$

$$\begin{cases} |\lambda_3| \left(\frac{\lambda_2}{\lambda_3}\right)^{\gamma_{23}} \left(1 + \frac{\lambda_1}{|\lambda_2|}\right)^{\gamma_{12}}, & \text{if } \lambda_1 \le 0, \lambda_2, \lambda_3 < 0 \\ |\lambda_3| \left(\frac{\lambda_2}{\lambda_3}\right)^{\gamma_{23}} \left(1 - \alpha\frac{\lambda_1}{|\lambda_2|}\right)^{\gamma_{12}}, & \text{if } \frac{|\lambda_2|}{\alpha} > \lambda_1 > 0 > \lambda_2, \lambda_3 \\ 0, & \text{otherwise.} \end{cases}$$

where $\lambda_1, \lambda_2, \lambda_3$ are the eigenvalues of the Hessian matrix at $\mathbf{x}$, while γ_{12}, γ_{23} control the sensitivity of the filter.

2.2.4. *Speed Function $\mathcal{F}_\mathrm{dir}$*

We introduce a new function $\mathcal{F}_\mathrm{dir}$ which depends only on the spatial relationship between voxel coordinates $\mathbf{x}(s)$, $\mathbf{x}_\mathrm{m}$ and $\mathbf{d}_\mathrm{m}$, but not on the intensities of an image, i.e., $\mathcal{F}_\mathrm{dir}$ represents our spatial *a priori* knowledge. Let $\mathbf{d} := \mathbf{x}(s) - \mathbf{x}_\mathrm{m}$, then $\mathcal{F}_\mathrm{dir}$ can be written as:

$$\mathcal{F}_\mathrm{dir}(\mathbf{d}, \mathbf{d}_\mathrm{m}) = f_\mathrm{dir}(\mathbf{d}, \mathbf{d}_\mathrm{m}) \cdot f_\mathrm{att}(\mathbf{d}), \quad (7)$$

where f_dir is the speed depending on the deviation of $\mathbf{d}$ from $\mathbf{d}_\mathrm{m}$, and f_att is an attenuation function. For f_dir, we propose the following Gaussian speed function:

$$f_\mathrm{dir}(\mathbf{d}, \mathbf{d}_\mathrm{m}) = \frac{1}{\sqrt{2\pi}\sigma} \exp\left(-\frac{\theta^2}{2\sigma^2}\right), \quad (8)$$

where θ is the angle between $\mathbf{d}$ and $\mathbf{d}_\mathrm{m}$:

$$\theta = \arccos\left(\frac{\mathbf{d}^T \cdot \mathbf{d}_\mathrm{m}}{\|\mathbf{d}\| \cdot \|\mathbf{d}_\mathrm{m}\|}\right). \quad (9)$$

With increasing distance from $\mathbf{x}_\mathrm{m}$, the influence of the prior is reduced to avoid unduly straight results. This is modeled using the following attenuation function f_att:

$$f_\mathrm{att}(\mathbf{d}) = \exp\left(-\frac{\|\mathbf{d}\|}{\alpha}\right). \quad (10)$$

Since $\mathcal{F}_\mathrm{v}$ and $\mathcal{F}_\mathrm{dir}$ are both isotropic, $\mathcal{P}_\mathrm{comp}$ is also isotropic. Thus, to find the minimum of (4), we can use the same numerical scheme as for (3), i.e., the upwind scheme [9], to solve the following extended Eikonal equation:

$$\|\nabla \mathcal{U}(\mathbf{x})\| = \mathcal{P}_\mathrm{comp}(s, \mathbf{x}_\mathrm{m}, \mathbf{d}_\mathrm{m}) + \epsilon. \quad (11)$$

3. EXPERIMENTAL RESULTS

To evaluate our approach, we used 10 high resolution 3D 7T MRA images of the region around the human lenticulostriate arteries. These images are acquired using a 3D gradient echo sequence with a repetition time of 15 ms, an echo time of 4.84 ms, a field of view of 135 × 180 mm, and a flip angle of 25 degrees. After applying isotropic interpolation, we have 128-162 slices in each 3D image. The size of the slices varies from 128×270 to 162×417 voxels, with a spacing of 0.23 mm. We

Table 1. Quantitative results for 510 gaps (errors in mm).

Approach	$\overline{e}_l < 0.3$	$\overline{e}_l < 0.4$	$\overline{e}_l < 0.5$	$\overline{e}_l < 0.6$	Total	Mean	p-Value	Avg. Run Time
FM-V	34.45%	61.22%	83.46%	92.72%	99.61%	0.406	< 0.00001	0.92 s
PROB [11]	56.69%	76.18%	86.61%	90.35%	96.65%	0.313	0.00085	51.68 s
Our approach	61.22%	86.42%	94.29%	97.64%	99.61%	0.288	–	1.63 s

have compared the results from our approach with those from a standard fast marching approach using a vesselness measure [7] (FM-V) and the probabilistic approach in [11] (PROB).

Fig. 3 shows the segmentation result for one 3D image. Fig. 3a,b demonstrates the advantage of our approach over FM-V when dealing with high curvature: the initial direction $\mathbf{d}_{\mathrm{m}}$ computed by the model-based approach is taken into account and consequently the transition between the segmentation from the two steps is smooth (Fig. 3b), while FM-V tends to find a short cut, resulting in an unnatural transition (Fig. 3a). Another example shows that PROB fails to complete a large gap (Fig. 3c), while our approach handles this case well (Fig. 3d). Fig. 3e shows the final result.

We quantitatively evaluated the results using manually created ground truth for 510 gaps in 10 3D images. For each centerline l of a gap, the error is determined (in mm) as

$$\overline{e}_l = \frac{1}{|l|} \sum_{\mathbf{v}_i \in l} |\mathbf{v}_i - \mathbf{v}_{\mathrm{gt},i}|, \tag{12}$$

where $\mathbf{v}_{\mathrm{gt},i}$ is the closest point of the ground truth to $\mathbf{v}_i \in l$. Table 1 shows the results of our approach along with a comparison with FM-V and PROB. Our approach leads to a higher number of completed gap centerlines closer to the ground truth (e.g., for $\overline{e}_l < 0.3$ mm we have 61.22%, compared to 34.45% and 56.69% for the previous approaches). Furthermore, a lower mean error of 0.288 mm compared to 0.406 mm (FM-V) and 0.313 mm (PROB) is achieved, and computed p-values from a paired t-test show that the difference is significant. Another advantage is that our approach is much more efficient than PROB, and only slightly slower than FM-V. The average run time for all gaps in one 3D image is 1.63 seconds (single-thread, 2.67 GHz CPU), while PROB [11] needs 51.68 seconds.

4. DISCUSSION AND CONCLUSIONS

We have developed a two-step approach for the segmentation of human cerebral vasculature from 3D 7T MRA images. We combine a model-based approach and a novel fast marching approach with anisotropic directional prior to achieve a fully automatic segmentation. Our approach has been successfully applied to high resolution 3D 7T MRA images. The experiments show that our approach is more accurate than two previous approaches, and it is computationally efficient.

Acknowledgment Support of the Deutsche Forschungsgemeinschaft (DFG) within the project QuantVessel (RO 2471/6) is gratefully acknowledged.

5. REFERENCES

[1] Z.-H. Cho, C.-K. Kang, J.-Y. Han, S.-H. Kim, K.-N. Kim, S.-M. Hong, C.-W. Park, and Y.-B. Kim, "Observation of the Lenticulostriate Arteries in the Human Brain In Vivo Using 7.0T MR Angiography," *Stroke*, vol. 39, no. 5, pp. 1604–1606, 2008.

[2] W. L. Nowinski, F. Puspitasaari, I. Volkau, Y. Marchenko, and M. V. Knopp, "Comparison of Magnetic Resonance Angiography Scans on 1.5, 3, and 7 Tesla Units: A Quantitative Study of 3-Dimensional Cerebrovasculature," *J. of Neuroimaging*, 2011, In press, published online.

[3] S. Wörz and K. Rohr, "Segmentation and Quantification of Human Vessels Using a 3-D Cylindrical Intensity Model," *IEEE Trans. on Image Proc.*, vol. 16, no. 8, pp. 1994–2004, 2007.

[4] N. D. Forkert, A. Schmidt-Richberg, D. Säring, T. Illies, J. Fiehler, and H. Handels, "Closing of Interrupted Vascular Segmentations: An Automatic Approach Based on Shortest Paths and Level Sets," in *Proc. SPIE Medical Imaging 2010: Image Processing*, San Diego, CA/USA, Feb. 2010.

[5] P. Lo, B. van Ginneken, and M. de Bruijne, "Vessel Tree Extraction Using Locally Optimal Paths," in *Proc. 7th IEEE Internat. Symposium on Biomedical Imaging: From Nano to Macro (ISBI'10)*, Rotterdam, The Netherlands, April 2010.

[6] V. S. Joshi, M. K. Garvin, J. M. Reinhardt, and M. D. Abramoff, "Identification and Reconnection of Interrupted Vessels in Retinal Vessel Segmentation," in *Proc. 8th IEEE Internat. Symposium on Biomedical Imaging: From Nano to Macro (ISBI'11)*, Chicago, Illinois, USA, March–April 2011.

[7] Y. Sato, S. Nakajima, N. Shiraga, H. Atsumi, S. Yoshida, T. Koller, T. Gerig, and R. Kikinis, "Three-dimensional multi-scale line filter for segmentation and visualization of curvilinear structures in medical images," *Medical Image Analysis*, vol. 2, no. 2, pp. 143–168, 1998.

[8] L.D. Cohen and R. Kimmel, "Global Minimum for Active Contour Models: A Minimal Path Approach," *Internat. J. of Computer Vision*, vol. 24, no. 1, pp. 57–78, 1997.

[9] F. Benmansour and L. D. Cohen, "Tubular Structure Segmentation Based on Minimal Path Method and Anisotropic Enhancement," *Int. J. of Comp. Vis.*, vol. 92, no. 2, pp. 192–210, 2011.

[10] S. Jbabdi, P. Bellec, R. Toro, J. Daunizeau, M. Pelegrini-Issac, and H. Benali, "Accurate Anisotropic Fast Marching for Diffusion-Based Geodesic Tractography," *Internat. J. of Biomedical Imaging*, vol. 2008, pp. 1–12, 2008.

[11] W. Liao, K. Rohr, C.-K. Kang, Z.-H. Cho, and S. Wörz, "A Generative MRF Approach for Automatic 3D Segmentation of Cerebral Vasculature from 7 Tesla MRA Images," in *Proc. 8th IEEE Int. Symposium on Biomedical Imaging: From Nano to Macro (ISBI'11)*, Chicago, Illinois, USA, March–April 2011.